ELSEVIER

Effect of Interfacial Properties on the Crack Propagation in Cementitious Composites

B. Mobasher* and Cheng Yu Li†
*Department of Civil and Environmental Engineering: Arizona State University, Tempe; and
†Vaughn & Melton Consulting Engineers, Asheville, North Carolina

The role of interfacial parameters on the fracture toughness of cement based composites are studied by means of a two-crack system. The first crack type represents the interfacial debonding of a fiber using a pullout model, while the second type simulates the crack growth in the matrix response subjected to the closing pressure generated by the fiber pullout force. A fracture mechanics approach is applied to the pullout of the short fiber. The interfacial zone is characterized as an elastic-perfectly plastic one-dimensional layer with a toughness lower than that of matrix or fiber. Stable debonding of fibers was modeled using R-curves so that the Interface toughness increases with an increase in debonded length. The closed-form solutions for strain energy release rate of a partially debonded frictional interface are solved for the critical debonding length. By obtaining the R-curve parameters, the fiber pullout load-slip response is simulated. The R-curve formulation is further applied to the crack growth in the composite. The toughening component is due to the closing pressure of fibers that depends on the matrix crack opening. The stress crack-width relationship is obtained as the crack growth in the stable region takes place. A parametric study of the effects of interfacial parameters on the crack growth in the composite is conducted. The present model is also compared with experimental data on the size effect in geometrically similar specimens. ADVANCED CEMENT BASED MATERIALS 1996, 4, 93–105

KEY WORDS: Closing pressure, Fiber bridging, Fiber reinforced concrete, Flexural response, Fracture properties, Pullout, R-curves, Size effect, Tensile strength, Toughening

High performance fiber reinforced cement based composite (HPFRCC) materials have received significant attention in the past decade. Development of these materials depends on a better understanding the interaction between the portland cement based matrix, fibers, and interface characteristics. This paper discusses the effect of interface properties on the fiber matrix debonding, and its eventual effect on the strength and strain capacity of the composite.

Several approaches are available to relate the fiber, interface, and matrix properties to the strength, toughness, and fracture properties of composite materials. Techniques based on fracture mechanics have been extensively used to model the interaction of the three phases on the ultimate response of composites [1]. The critical volume fraction of fibers necessary for distributed cracking has been studied using an energy balance criterion by Li et al. [2,3] and Naaman [4]. Tjiptobroto and Hansen [5] also used an energy balance approach to compute the strain at the end of multiple cracking region. Strengthening of the matrix phase and the critical volume fraction of fibers have been studied using a micromechanics approach [6,7]. Mobasher and Li [8] used short whiskers with a high aspect ratio to strengthen the composite at the micro level.

The frictional sliding of fibers is considered as the main component of reinforcement in fiber reinforced cement (FRC) materials. The frictional shear strength has been used as a closing pressure that is inversely proportional to the crack width. Using pullout experiments under closed-loop conditions, the interfacial region was modeled by Li et al. [9]. As the fiber debonds, stiffness of the pullout force versus slip decreases, resulting in the nonlinear response of the ascending part of the pullout curve. To simulate the changes in specimen compliance and characterize the pullout-slip response, nonlinear fracture models based on R curves have been recently used [10,11].

Cement based composites exhibit the general characteristics of brittle matrix composites, whereas the failure of the matrix precedes the fiber failure. When sufficient fibers are present to carry the load released by the matrix, composite toughening may take place due to processes such as fiber bridging. The magnitude of toughening is therefore dependent on the interaction of the fiber, matrix, and interface. In the present approach, transverse cracking of the matrix phase is considered as the single mode of failure as shown in Figure 1. Propa-

Address correspondence to: Barzin Mobasher, Department of Civil and Environmental Engineering, Arizona State University, College of Engineering and Applied Sciences, Tempe, Arizona 85287.
Received November 29, 1995; Accepted July 24, 1996

ISSN 1065-7355/96/$15.00
PII S1065-7355(96)00073-9

Advn Cem Bas Mat
1996;4:93–105

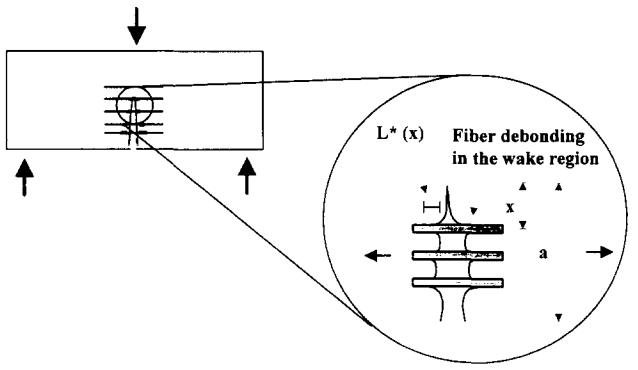

FIGURE 1. Schematics of fiber debonding in the wake region and the two-crack system representing the matrix crack and the debonding zone.

gation of a matrix crack results in debonding of the fibers. The pullout force of the fiber increases with debonding, resulting in crack closure and a decrease in the stress intensity factor at the crack tip. Further growth of the matrix crack depends on the closing pressure and the extent of fiber debonding in the wake region.

The principle of superposition has been commonly used to combine the contribution of fibers to the crack growth resistance of matrix. Stress-crack width relationships are commonly used to characterize the tension-softening response [12,13]. The form of these functions is obtained from the descending branch of the stress-displacement curves in a uniaxial tension test. To consider the evolution of the process zone prior to the steady-state conditions, the present approach considers the gradual fiber debonding to allow for the crack opening.

Model Description

In the proposed method, a single fiber pullout slip model is used as the closing pressure formulation over the stable crack growth region. Propagation of the matrix crack leads to its further opening, thus promoting the growth of the debonding zone in the wake of the main crack. For a given crack opening, interface properties are used to compute the pullout force. The fiber pullout force distribution is computed iteratively based on the equilibrium crack opening as a function of the specimen geometry, far-field applied load, debonding length of fibers, and the interface properties. This process is repeated for every increment of matrix crack growth.

A composite specimen is idealized as having a series of straight, aligned, short fibers of constant length in the path of the matrix crack. This approach is chosen to show the formulation of present model using a single fiber pullout. This assumption, although not realistic for a random distribution of fiber lengths, lends itself to more refined approaches utilizing Monte-Carlo simulation. Alternatively, one can use the results of an inclined fiber pullout test as conducted by Ouyang et al. [10] as the constitutive response. Fiber parameters include stiffness, length, diameter, and volume. Interface properties are defined using frictional and adhesional strength, fracture toughness, and stiffness. The quasi-linear fracture properties of matrix are defined using the two-parameter fracture model of Jenq and Shah [14] and its *R*-curve simulation as described by Ouyang et al. [12].

A general *R*-curve approach is used to model stable growth of the two-crack systems consisting of both the matrix crack and the fiber interface crack. Defined as the locus of fracture energy release rates, *R*-curve formulations relate the stable crack growth to the increase in the apparent fracture toughness of a material as shown in Figure 2. Conditions for unstable growth of the matrix or interface crack are stated as:

$$R = G, \frac{\partial R}{\partial a} = \frac{\partial G}{\partial a}. \tag{1}$$

It is shown by Ouyang et al. [15] that the *R*-curve can be derived as:

$$R(a) = \beta \left[1 - \frac{d_2}{d_1} \left(\frac{\alpha a_0 - a_0}{a - a_0} \right)^{d_2 - d_1} \right] [a - a_0]^{d_2} \tag{2}$$

$$d_i = \frac{1}{2} + \frac{\alpha - 1}{\alpha} \pm \sqrt{\frac{1}{4} + \left(\frac{\alpha - 1}{\alpha} \right)^2}, \; i = 1,2 \quad \alpha = \frac{a_c}{a_0}. \tag{3}$$

The parameters of the *R* curve that are referred to as α and β depend on the strain energy release rate of the geometry considered and the failure criteria used. This approach is applied to both the three-point bend and the fiber pullout.

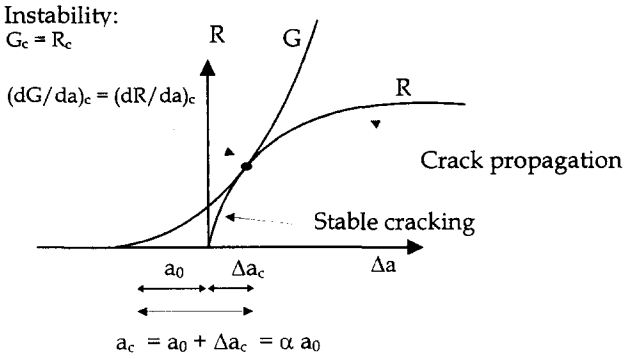

FIGURE 2. The *R*-curve model used for the growth of the matrix crack and the debonding zone.

Fiber Debonding and the Pullout Slip Response

Growth of debonding zone is modeled as a mode II crack in the elastic-perfectly plastic one-dimensional layer interface. A formulation based on a shear lag approach by Stang et al. [16] was used. Schematics of the model and the constitutive response of the interface are shown in Figure 3 using an elastic fiber of length L, which is partially debonded along length L^*, a rigid matrix, and an elastic-perfectly plastic interfacial zone. The fiber perimeter is defined as $\Omega = 2\pi r$. The interface is characterized by its shear stiffness K, adhesional bond strength q_y, frictional sliding strength q_f, and the interface toughness Γ_i. Strain energy release rate of a partially debonded frictional interface as expressed by Stang et al. is:

$$G = \frac{1}{2E_f A\omega\Omega}\left[\frac{dP^*}{dL^*}q_f L^*\chi - (P^{*2}\chi^2 - q_f L^*)(P^* - q_f L^*)\omega - P^* q_f \chi\right] \quad (4)$$

$$\omega = \sqrt{\frac{K}{EA}} \qquad \chi = \coth(\omega(L - L^*)). \quad (5)$$

Substitution of eqs 2 and 4 in the crack growth criterion of eq 1 results in two second-order differential equations for the pullout force:

$$\frac{dP^*}{dL^*} = \frac{1}{q_f L^*\chi}[2E_f A\Omega\omega R(L^*) + \omega P^{*2}\chi^2 - \omega P^*\chi^2 q_f L^* - \omega P^* q_f L^* + P^* q_f \chi]$$

$$\frac{d^2P^*}{dL^{*2}} = \left[2E_f A\Omega\omega\frac{dR}{dL^*} - (s^2 - \chi^2)q_f L^*\omega + 2P^*\omega\chi^2 - \omega q_f L^*\right] + \frac{1}{q_f L^*\chi}[2E_f A\Omega\omega R(L^*) + (P^*\chi^2 - q_f L^*)(P^* - q_f L^*)\omega + P^* q_f \chi] - \frac{1}{q_f L^*\omega}[2P^{*2}\omega^2\chi s^{-2} - P^* q_f \omega(1 + \chi^2 + 2L^*\omega\chi s^{-2} + s^{-2})\, 2L^* q_f \omega] \quad (6)$$

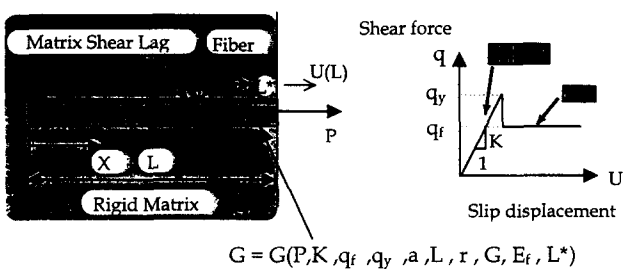

FIGURE 3. The fiber pullout model used as a closing pressure distribution.

Where $s = \sinh(\omega(L - L^*))$. These equations are solved numerically as two first-order initial value problems. The first initial condition assumes that the fiber force at the initiation of the debonding is zero. Such an approximation is necessary since Steif and Dollar have shown that a linear elastic fracture mechanics (LEFM)-based fracture approach requires an infinitely large debonding initiation load [17]. The second initial condition assumes that an infinitesimal yielding of the interface is necessary for crack propagation. The rate of change of load at the onset of interface yielding is also used as the initial condition:

$$P^*(L_0^*) = 0, \quad \frac{dP^*}{dL^*} = q_f - q_y \cosh^{-2}(\omega(L - L^*)) \;@\; L^* = L_0^*. \quad (7)$$

The solution of these equations requires knowledge of the R curve, which must be determined first. The shape of the R curve is defined in terms of two unknowns α and β, which represent the effect of materials and geometry. The algorithm for determination of the R curve is described next. The R curve is assumed to start from zero, that is, material has no resistance to initiation of cracks, however, the toughness increases during the initial few debonding increments. The critical condition takes place at the point where the steady-state cracking conditions are satisfied, $G = R = \Gamma_i$, where Γ_i represents the interface fracture energy. This criterion defines the plateau value of the R curve.

$$R(L_c^*) = G(L_c^*) = \Gamma_i, \quad \frac{\partial R}{\partial L^*} = \frac{\partial G}{\partial L^*} > 0 \;@\; L = L_c^* \quad (8)$$

A second criterion is needed to define the critical length of debonding, or L_c^*. It is prescribed that the maximum load takes place at the critical crack length, which also corresponds to the tangency of the G and the R curves. This condition, however, cannot be used as an initial condition. The shooting method [18] is used to transform the boundary value ordinary differential equation (ODE) into a first-order ODE by assuming a critical debonding length, L_{ci}^*. Parameter α is then obtained as L_{ci}^*/L and used with the condition $R\,(L_{ci}^*) = \Gamma_i$ to compute the parameter β. With a knowledge of α and β, the differential equations for the pullout force as a function of debonded length (eqs 6 and 7) are then solved using a fourth-order Runge-Kutta approach, which is an unconditionally stable predictor-corrector method. The R curve is constructed and used in eq 6 to solve for the load necessary to extend the debonded crack at that assumed level. The procedure is repeated and the critical debonding length L_{ci}^* is computed iteratively to correspond to the maximum load. This procedure is explained in detail in ref 11.

At each increment of interface debonding, the up-

Advn Cem Bas Mat
1996;4:93–105

dated load is used to calculate the fiber slip. Once the steady-state conditions of eq. 8 are achieved, the crack is allowed to propagate under constant fracture toughness Γ_i, that is, the R curve is replaced by a single parameter toughness as proposed by Ouyang et al. [15,19] and Bazant and Kazemi [20]. As the fiber debonds completely, the load decreases to allow for constant energy release rate. Similar to the work of Marshall [21], a frictional pullout response was used for the completely debonded fiber. This assumption neglects the effect of slip, Poisson's contraction, and residual stresses.

Effect of fiber length on the closing pressure constitutive response is shown in Figure 4a and b. Stable debonding is modeled by the incremental increase in the interfacial toughness as shown in the R curve plot of Figure 4a. A constant initial debonded length L_0^* of 0.2 mm is assumed. Unless specified, a constant value of interface toughness of Γ_i = 0.0011 N/mm obtained from experimental data of Li et al. [9] was used for the parametric studies. As the fiber length increases, the extent of stable crack growth and load-carrying capacity increase. The load-slip response is shown in Figure 4b. Note that stable debonding continues up to approximately 80% the length of the fiber. As the fiber length increases, the R curves converge toward a master R curve, indicating that the geometrical effects become negligible. The master curve ascends to the constant prescribed interface toughness used for the cement based materials. The pullout force is maximized when the R curves reach the plateau level. Ultimate pullout force increases with an increase in the fiber embedded length.

The present model for debonding can be compared to the experimental results of pullout tests. Pullout responses of steel fibers are shown in Figure 5. Effect of interfacial parameters such as the stiffness ω, adhesional and frictional shear strength q_y, q_f, and the specific surface fracture energy Γ_i can be observed in the ascending portion of the load-slip response. Stiffness of the interface ω contributes to the slope of the ascending portion in its linear range. The adhesional bond strength q_y controls the initiation of debonding. The peak load is dependent on the fiber length, interface shear strength q_f, and fracture toughness. It is shown that from 14 to 28 days of curing, the changes that take place in the pullout slip response may be modeled by an increase in the adhesional and frictional bond strengths (q_y, q_f) from 0.44 and 0.31 N/mm to 1.6 and 1.0 N/mm, respectively. The present model predicts the initial stiffness of the pullout slip response and the maximum load quite accurately; however, it overestimates the experimental results in the frictional pullout range. This may be due to dissipative mechanisms other than the constant frictional shear assumed in this case.

Fracture of the Composite

The strain energy release rate for a three-point bending specimen is obtained from the stress intensity factor handbook [22]. K_{IP} is given by:

$$K_{IP} = \frac{3s\,P\sqrt{\pi\alpha_m}}{d}\,g(\alpha_m), \qquad \alpha_m = \frac{a_m}{d}, \text{ and} \tag{9}$$

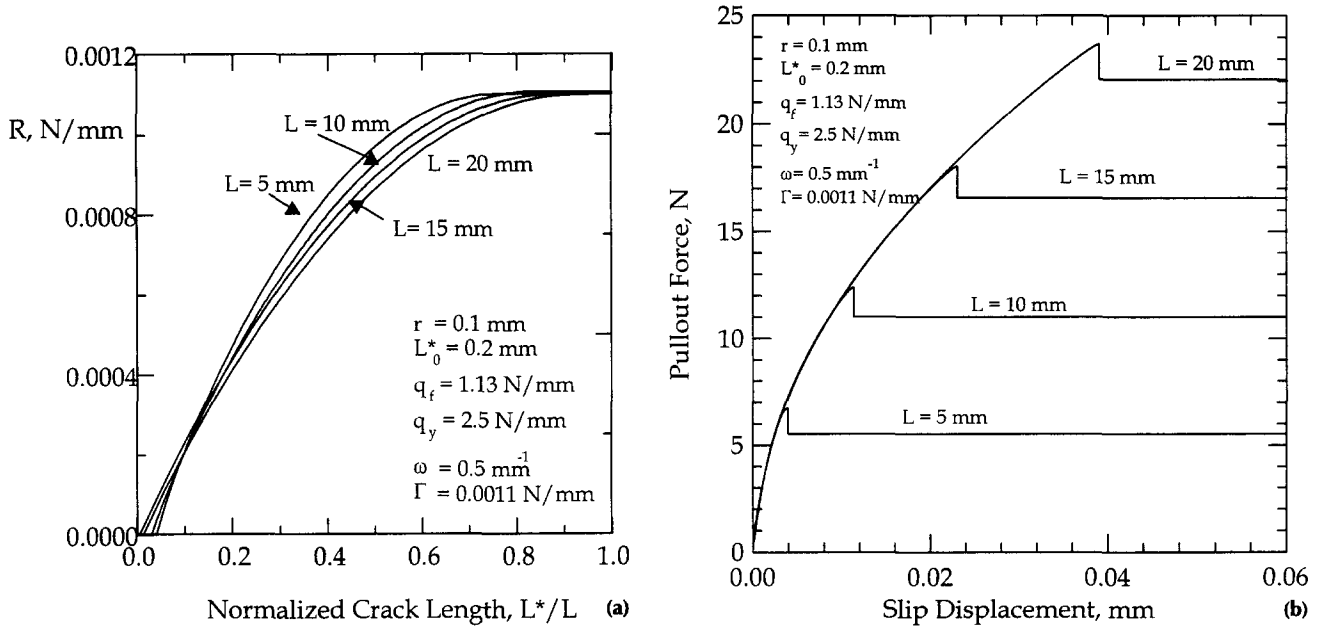

FIGURE 4. Effect of fiber length on the fiber pullout response. (a) The R curve versus debonded length. (b) Force versus slip response used as the closing pressure constitutive model.

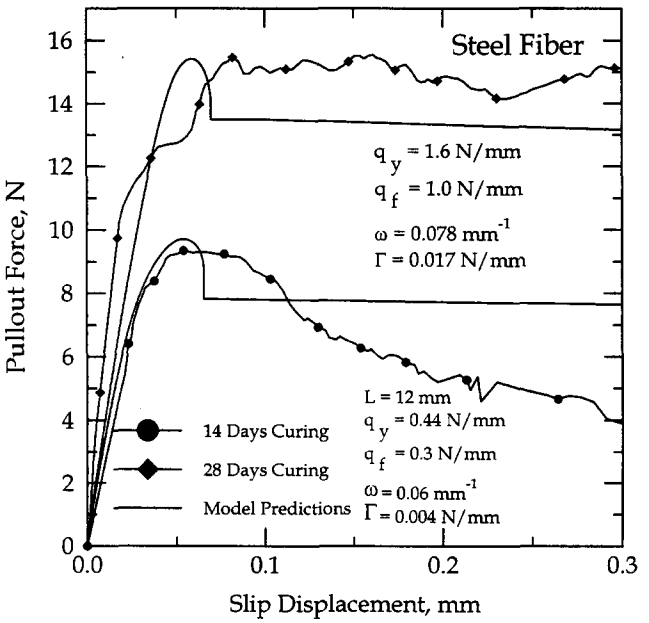

FIGURE 5. Pullout force versus slip model predictions for steel fibers subjected to 14 and 28 days of curing. L = 12 mm.

$$g(\alpha_m) = \begin{cases} \dfrac{1.99 - \alpha_m(1-\alpha_m)(2.15 - 3.93\,\alpha_m + 2.7\,\alpha_m^2)}{2\,b\,\sqrt{\pi d}\,(1+2\alpha_m)(1-\alpha_m)^{3/2}} & s/d = 4 \\ \dfrac{(1.0 - 2.5\alpha_m + 4.49\alpha_m^2 - 3.98\alpha_m^3 + 1.33\alpha_m^4)}{2bd(1-\alpha_m)^{3/2}} & s/d = 2.5 \end{cases}$$

where s represents the span, P the far-field load, d the beam depth, a_m the matrix crack length, and b the specimen width. Using Irwin's approximation, the strain energy release rate of the composite can be expressed as:

$$G = \frac{(K_{IP} + K_{IF})^2}{E'} \tag{10}$$

where $E' = E$ for plane stress and $E' = E/(1 - \nu^2)$ for plane strain conditions. K_{IF} represents the closing pressure of the fibers and will be discussed in the following section.

An elastically equivalent crack approach is used. The closing pressure distribution can be modeled by integrating the pullout force across the crack face. The reduction in stress intensity factor can be obtained by using the stress intensity due to a unit load over the crack length. The crack opening displacement (COD) for an edge crack subjected to a unit force was used as the Green's function [23]. The effect of fibers that close the crack faces and reduce the stress intensity factor may be expressed as:

$$K_I^e = K_{IP} - \int_0^a \phi\, P^* \left(\frac{COD(x)}{2}\right) g\left(1, \frac{x}{a}\right) dx \tag{11}$$

$$COD(x) = COD_p(x) - \frac{2}{E'}\int_0^a \int_x^a \phi P^*\,(COD(\xi)/2)\, K_{IP}^*\left(1, \frac{\xi}{a}\right) \frac{\partial K_{IF}^*\left(1, \frac{\eta}{a}\right)}{\partial F} d\,\eta\, d\xi \tag{12}$$

where K_{IP} and COD_P are the stress intensity factor and crack opening profile for an effective traction-free crack in the matrix due to far-field stress. The first terms in these equations represent the elastically equivalent fracture properties of the matrix phase. The second terms are due to the closing pressure of fibers and represent the summation of contributions from fibers along the surface of the crack. Parameter ϕ represents the averaging factor to convert a single fiber pullout force to a distributed pressure acting on the crack face. It was defined as a function of fiber volume fraction normalized with respect to the effective area of the specimen, $\phi = \lambda V_f/\pi r^2$, where V_f represents the volume fraction of fibers. Parameter λ represents the effect of fiber orientation and length distribution according to Aveston and Kelly [24] and was set equal to 1 for the present approach. The expression for the function $g(1,x/a)$ is discussed in the Appendix. A single fiber located at point ξ along the crack causes displacements along the entire crack surface. Castigliano's theorem is used in the calculation of the crack opening. Note that x is the distance from the specimen edge to the point of applied unit force on the crack faces. The inner integral in the second term of eq 12 computes the contribution of the fiber located at ξ to the closing of the crack. The independent variable η represents various points along the crack surface at which a displacement due to the force applied at point ξ is obtained.

The constitutive relationship between the pullout force of a fiber as a function of slip, $P^*(u)$, is obtained from the previous section. This response is used as the stress crack width response, $P^*(COD(x)/2)$, and represents the closing pressure distribution as a function of crack opening. For every embedded length, one pullout slip response is required. For a random distribution of fiber lengths, the approach would require development of the density function of the pullout responses and use of $P^*(u)$ as a random variable. To simplify the solution algorithm, we used the assumption of constant length of fibers across the crack to justify use of a single fiber length.

Instability conditions for the composite are defined using two criteria of a critical stress intensity factor, and the crack opening displacement at the tip (CTOD) of a fictitious crack. These equations are stated in terms of two unknowns, the critical crack length and critical far-field load, and expressed as:

$$K_I^e = K_{Ic}^S \tag{13}$$

$$COD(a_0) = CTOD_C \tag{14}$$

These two coupled integral equations are solved using numerical methods. Using an iterative procedure, the critical crack is increased incrementally from the initial crack length a_0. Due to the existence of the notch, the first iteration assumes that no fiber is present in the crack path. As the crack length is incrementally increased, the LEFM crack opening profiles are used as the initial starting point for the estimation of pullout force. The load applied to the composite and the closing pressure distribution are obtained by solving the nonlinear equations. For an assumed crack length, $a^i > a_0$, the load calculated from the stress intensity criterion is given by:

$$p_1^{i+1} = \frac{K_{Ic}^S + K_{IF}(p_1^i)}{K_{IP}|_{P=1}} \tag{15}$$

where i represents the increment number. The load calculated from eq 14 is given by:

$$p_2^{i+1} = \frac{CTOC_c + CTOD_f(p_2^i)}{CTOD_p|_{P=1}}. \tag{16}$$

These two loads p_1^{i+1} and p_2^{i+1} are compared, and if the tolerance criteria are not met, a new crack length is assumed and the procedure is repeated. Otherwise, if they are within the prescribed tolerance, it is assumed that the critical crack has reached and the maximum load is taken as the average of the two loads. In the numerical examples presented next, a tolerance of 2 N between p_1 and p_2 was used.

The solution results in a far-field load, P_{max}, and the length of stable crack extension, a_c, at the moment the critical conditions are satisfied. The closing pressure of the fibers and the debonded length distribution across the crack faces are also computed using the fiber slip response. To simulate the load-CMOD response of the sample, the R curve for the composite can be defined by using the values of a_c and P_{max} in eq 9 to obtain the parameters α and β of the composite R curve.

$$\alpha = \frac{a_c}{a_0}; \tag{17}$$

$$\beta = \frac{(K_{Ic}^S + K_{IF}(P_{max}))^2}{E'\left(1 - \frac{d_2}{d_1}\right)(a_c - a_0)^{d_2}} \tag{18}$$

Note that K_{Ic}^S in eq 18 is the critical stress intensity factor of the matrix, which includes the effect of aggregate interlock on the fracture process zone. The R curve obtained underestimates the composite toughness, because the fracture process zone in the real composite is likely larger than that of plain matrix. The present approach assumes that the material properties of the matrix K_{Ic}^S and $CTOD_c$ are unaffected by the presence of fibers. This approach does not modify the length of the process zone due to the existence of fibers, and it is assumed that the bridging force is effective on the quasibrittle materials' cracked ligament.

Once the parameters of the R curve are defined, the simulation of load-CMOD response can be achieved by an incremental approach. The crack length is increased, and the R curve is used to compute the toughness. This value of the toughness is used to compute the force necessary for the condition $G(a_i) = R(a_i)$, where a_i represents the increment of crack. Note that since the fiber closing pressures are already incorporated in the R curve formulation, the specimen is treated as an elastically equivalent material. For the crack propagation beyond the ultimate load, the toughness of the composite is modified to account for the additional term due to the crack growth beyond the critical length. This can be defined in terms of the K^R curve as shown in eq 19. The first term is accounted for by the R-curve model. The second term represents the crack growth beyond the critical length and includes an additional closing pressure due to the growth of the crack.

$$K^R = \begin{cases} \sqrt{E'\,R(a)} & a \leq a_c \\ \sqrt{E'\,R(a_c)} + K_{IF}(a) - K_{IF}|_{a=a_c} & a > a_c \end{cases} \tag{19}$$

Crack Opening Profiles and Bridging Force Distributions

The bridging force develops as the matrix crack propagates and opens in the process. In the present formulation, fiber interfacial parameters can be directly related to the toughening mechanisms. A three-point bend specimen with dimensions of 25.4 × 76.2 × 330.2 mm and an initial notch length of a_0 = 19.05 mm was used for the parametric study. No fibers are present in the initial notched region. An FRC composite with 10% steel fibers that are 20-mm long is compared to a plain mortar matrix with a traction-free crack. It is assumed that the matrix crack intersects the fibers at their midpoint. A 10-mm length of fiber was used to generate the pullout slip response.

Crack opening profiles corresponding to three intermediate crack lengths of a = 19.5, 21.5, and 23.8 mm are shown in Figure 6a. The magnitude of the point load for these cases is sufficient to cause the net stress intensity factor at the crack tip to be equal to the critical value K_{Ic}^S. This would simulate the onset of crack growth at the specific length. As the crack propagates, the contribu-

tion of fibers increases. For instance, as compared to a traction-free crack, the COD at the initial tip is as much as 18%, 40%, and 55% smaller. As the crack propagates, the shape of the crack opening profile and the distribution of traction forces along the crack surfaces change. In the present case, the stress-crack width relationship depends primarily on the ascending region of pullout slip response. This approach is different from other methods that use postpeak strain-softening curve obtained from a uniaxial tensile test in the form of σ-ω constitutive response.

The bridging force distributions on the crack faces corresponding to the three crack lengths are shown in Figure 6b. The distribution of the bridging forces are similar to the crack opening profiles, because the closing pressure is in the ascending range of the pullout slip response. The present formulation assumes that the initial stress at the fibers was zero. To generate the pullout force in the fibers, an infinitesimal crack opening is required. It is possible that the load in the composite is maximized while the crack opening magnitude is still limited to the ascending portion of the fiber pullout response. In such a case, the adhesional bond strength of the interface plays a dominant role in the response of the specimens.

To investigate the matrix parameters that control the extent of crack growth, we studied two identical specimens with 5% steel fibers. The difference between these two specimens is in the prescribed value of $CTOD_c$ to simulate the effect of stable crack growth length. One can expect a longer crack length in a material with larger $CTOD_c$. Two values of $CTOD_c$ equal to 0.02 and 0.025 mm are used. Figure 7a represents the load-crack mouth opening displaced (CMOD) response of both specimens as compared to the cases of no fiber composites. Note that the strength of both materials are increased by the addition of fibers. The associated increase in the ultimate strain capacity is also shown. The postpeak response of plain mortar specimens are descending, whereas the fiber composites exhibit a higher degree of ductility beyond the peak load. The crack opening profiles at the onset of peak load are also shown in Figure 7b. The stable crack length increases with increasing $CTOD_c$. The fiber debonded lengths are shown in Figure 7c. In the case of $CTOD_c$ = 0.025 mm, the fiber at the vicinity of the initial notch is debonded entirely and the frictional stress provides a constant closing pressure. In the vicinity of the crack tip, the fibers are partially debonded and the bridging force is less than the maximum pullout force. The closing pressure distribution is shown in Figure 7d. The shape of the closing pressure distribution is directly obtained from the fiber debonding profile. Both the interface bond strength and frictional shear strengths are operative at the crack opening profiles studied in the present case.

Parametric Study

The present approach may be used to separate out the contribution of the fibers in reducing the stress intensity factor of the composite. This is achieved by comparing

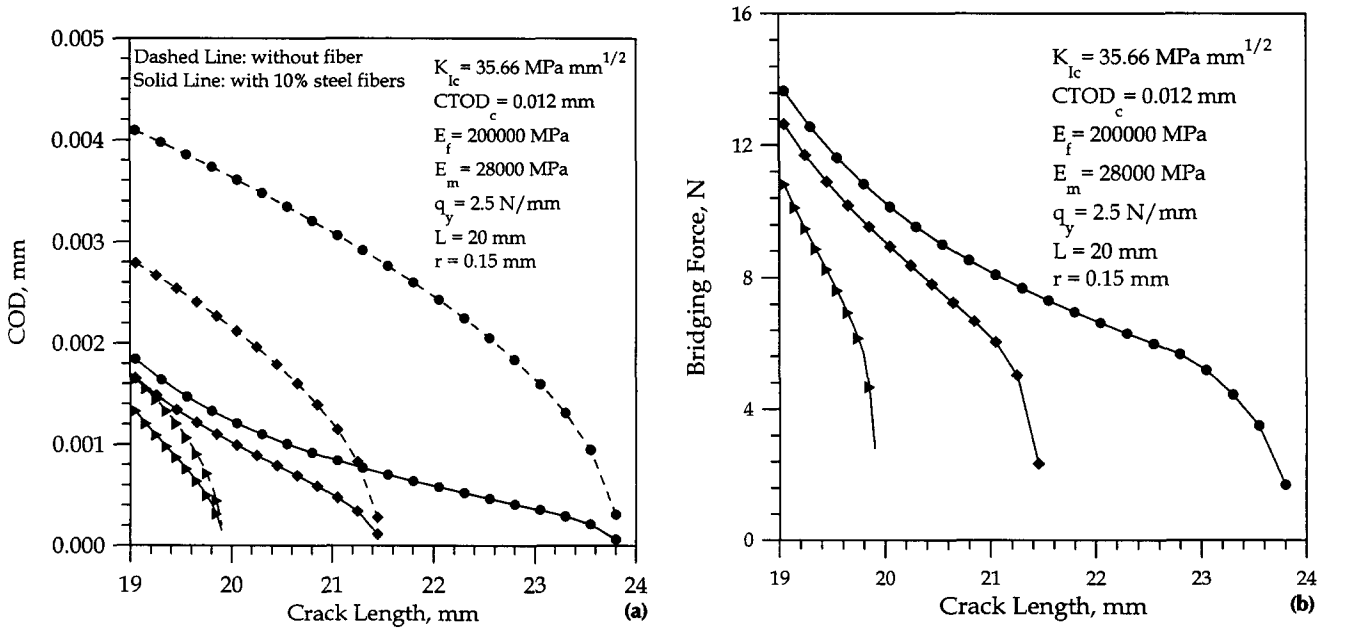

FIGURE 6. (a) Crack opening profile as compared to linear elastic fracture mechanics values for three intermediate lengths in the stable crack growth region. (b) The bridging force distribution. COD = crack opening displacement; CTOD = crack tip opening displacement.

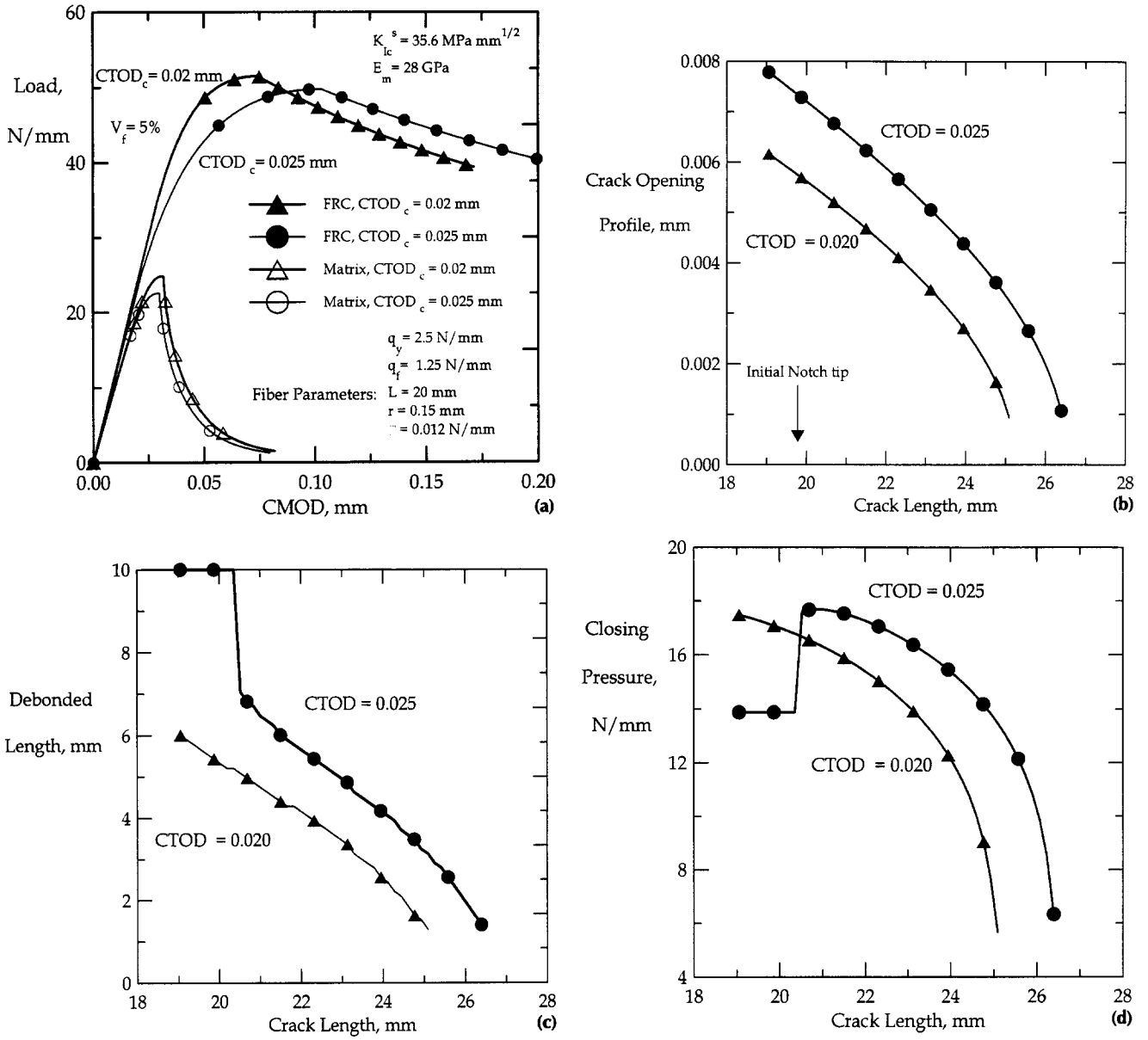

FIGURE 7. (a) The load-crack mouth opening displacement (CMOD) response of composites with 5% steel fibers compared to matrix phases for two levels of $CTOD_c$. (b) The crack opening profile at the point of maximum load. (c) The debonded length in the wake region. (d) The closing pressure distribution. CTOD = crack tip opening displacement; FRC = fiber reinforced concrete.

the relative contributions of the two stress intensity parameters plotted on a normalized load-deflection response of a composite as shown in Figure 8a, b. The relative contribution of the stress intensity applied by the far-field load and the stress intensity removed due to the closing pressure is shown in Figure 8a. The load taken by the composite includes the contributions of matrix and fibers. These load ratios are calculated based on the relative contribution of each phase to the stress intensity factor. It is observed that before the matrix crack propagation begins, the majority of the load is mainly taken by the matrix. As the overall load on the composite is increased, a major portion of the force is transferred to the fibers, and fiber bridging becomes the dominant load-carrying component of the system. Crack propagation in the matrix proceeds with a decreasing load. After the matrix cracks, contribution of fibers increases rapidly. In the postpeak region, matrix's contribution decreases and the major toughening and load-carrying capacity of the composite is due to the fibers.

The relationship between the closing pressure, crack

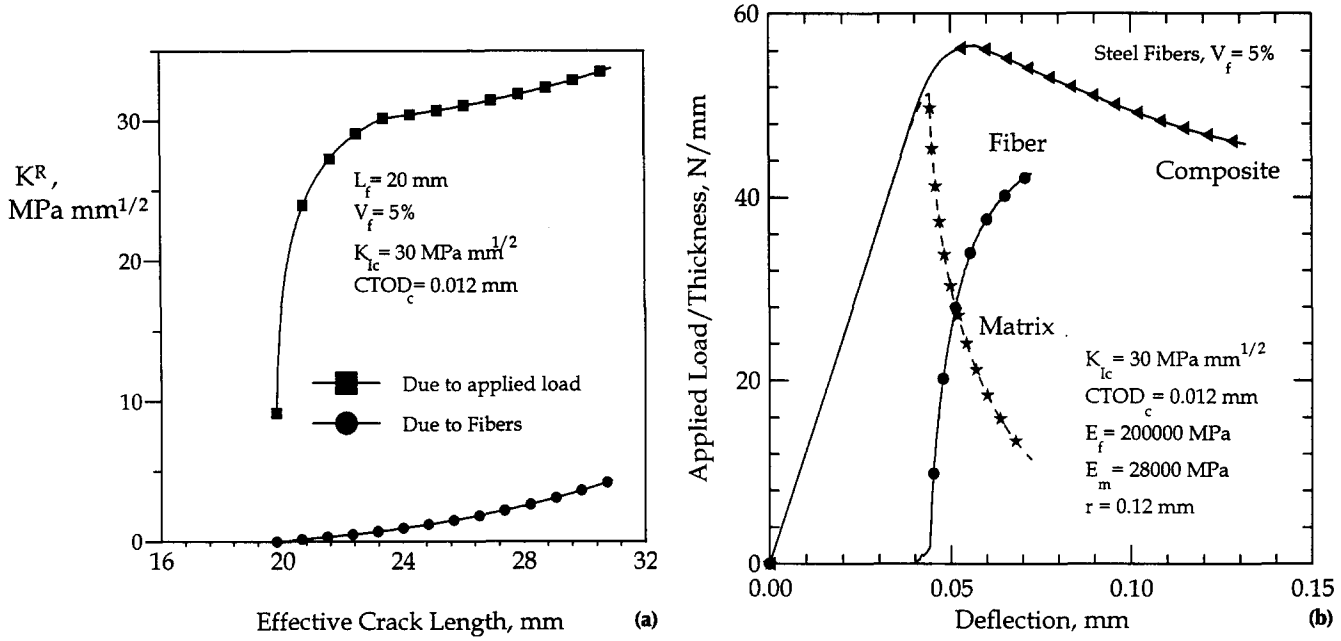

FIGURE 8. Relative contribution of the stress intensity by the far-field load, and the stress intensity removed by the closing pressure. (b) The normalized load-deflection response. The load taken by the composite includes the contributions of matrix and fibers. CTOD = crack tip opening displacement.

opening profile, and the toughening is studied next. Effect of interfacial shear strength q_y on the crack opening profiles and the K^R curves is shown in Figure 9a and b, respectively. As the interfacial shear strength increases, the stiffness of the pullout force versus slip displacement increase, and the fibers provide higher bridging forces at the same crack opening level. It is shown that as the interfacial shear strength increases from 2.5 N/mm to 5.5 N/mm (an increase of 120%), the bridging force increases by 15%.

For a constant prescribed length of fibers, the effect of varying fiber volume fraction on the K_R curves of com-

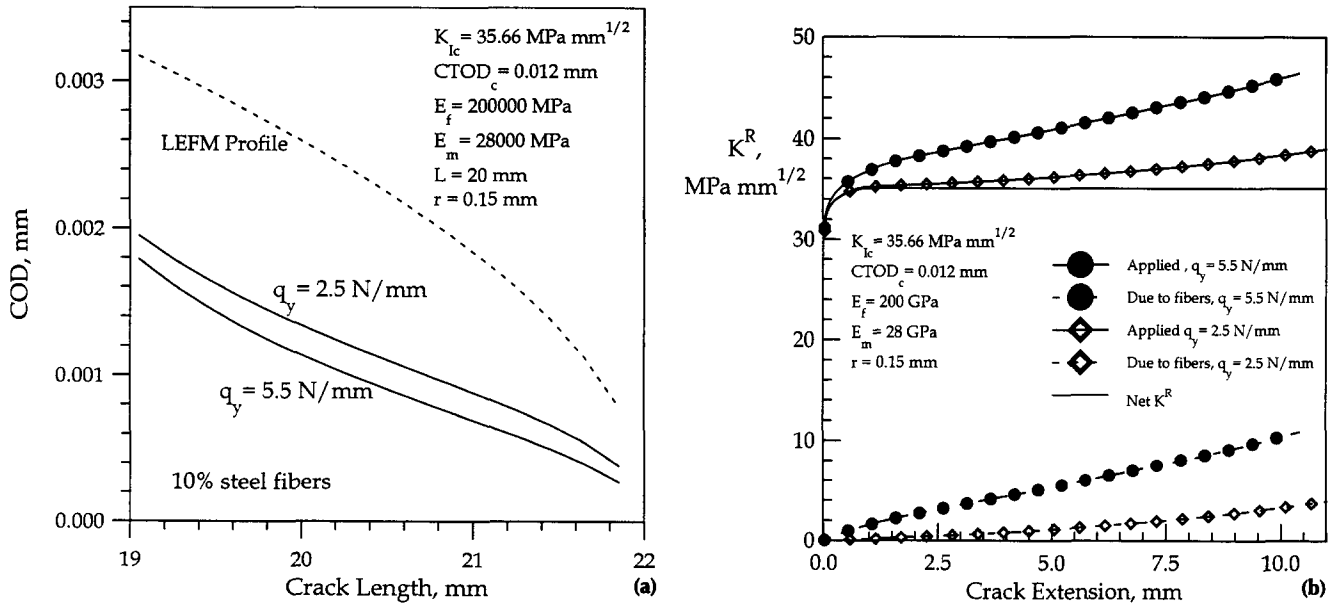

FIGURE 9. (b) Effect of interfacial shear strength q_y on the crack opening profiles. (b) The K^R curves as a function of q_y. COD = crack opening displacement: CTOD = crack tip opening displacement.

Advn Cem Bas Mat
1996;4:93–105

posites is shown in Figure 10. Because the fiber length is maintained constant, the scaling parameter ϕ increases as the fiber fraction is increased. The pullout force increases proportional to the parameter ϕ resulting in an increase in the ascending rate of the K^R curve for the composite. This is shown in Figure 10a. The force versus deflection response of the composite is obtained from the K^R curve and is shown in Figure 10b. Both the load and deflection at the maximum load of the flexural specimens increase due to an increase in the fiber content. At the volume fraction corresponding to 12%, the closing pressure distribution is sufficient to carry the load released due to the cracking of the matrix. It is observed that the specimen behaves in an elasto-quasiplastic response. This behavior has been observed in the experimental results of various researchers and indicates the ability of the present approach in predicting the multiple cracking region. The effect of increasing the specific surface area on the strength of the composites was first shown by Romauldi and Batson [25].

According to the present approach, as long as the crack opening level is in the ascending part of the pullout response, the effect of fiber length on the crack profile, hence, the bridging force, is not significant. However, as the fiber debonds completely and the frictional pullout mechanisms become operative, the effect of fiber length becomes a dominant factor. This is shown in Figure 11 that presents the effect of fiber length on the maximum load carried by the composite. It is shown that as the fiber length increases, the peak load increases. For a constant number of fibers intersecting the crack, increasing the fiber length increases the potential pullout length, thereby increasing the closing pressure distribution. Parameter P_{cu} represents the ultimate load for the composite and is normalized with respect to matrix ultimate load defined as P_{mu}. Parameters α and β define the R curve for the cases presented. As the fiber length increases, parameter β, which characterizes the plateau level of the R curve, increases. Parameter α is defined as the crack length at failure normalized with respect to the initial notch length; it decreases as the fiber length increases. This indicates that the crack growth in a material is being opposed with the added resistance offered by the fibers of longer length. The critical load is achieved at much higher loads but at reduced levels of effective crack lengths. Similar observations were made by Bryars et al. [26] in the size-effect analysis of the FRC composites and Mobasher et al. [23].

The present approach provides a direct method of correlation between fiber interface, length, bond strength, and fracture toughness with the macroscopic fracture properties of the composite. Theoretical measures of proportional elastic limit (PEL) and modulus of rupture (MOR) can be easily defined and compared with the equivalent elastic definitions.

Size Effect in Fiber Reinforced Concrete

A recent study of size effect in FRC conducted by Bryars et al. [26] was considered in the present approach. The experimental results were based on three-point bending specimens subjected to closed-loop testing under a controlled flexural crack growth. The mixture was a high strength concrete mixture with nominal aggregate size of 12 mm, a water:cement ratio of 0.35, and a microsilica:cement ratio of 0.1. Straight steel fibers were used at a constant volume fraction of 0.5%. Two different fiber lengths of 6 mm and 13 mm were used. Results are compared to ordinary concrete tested under the same conditions. Three different sizes of geometrically similar specimens with a constant thickness of b = 50 mm; depths of d = 80, 160, and 320 mm; and span of 2.5 d were studied. Notch depths of 0.275 d were cut using a water-cooled diamond saw.

The stress intensity factor for this specimen was obtained from Gettu et al. [27] and was presented earlier in eq 9. In the present work, the load versus CMOD of the specimens is used as a measure of the fit. The material properties were obtained from typical values used for matrix based on the two-parameter model and the size-effect law after evaluating the range of values provided by various researchers. For the specimens studied in the present work, a constant critical stress intensity factor equal to 40.5 MPa $mm^{1/2}$ was used. This value is lower than the number reported by Bryars et al. of K_{Ic} = 53.5 MPa $mm^{1/2}$ obtained based on the size-effect law. The following equation provided by Shah et al. [28] was used to convert the process zone lengths for an infinitely large specimens (c_f) to $CTOD_c$.

$$CTOD_c = 2.854 \sqrt{\frac{G_f}{E}\left(0.081a_0 + c_f - \frac{0.081a_0^2}{a_0 + c_f}\right)} \qquad (20)$$

Based on the Bryars et al. data, values of E = 36600 MPa, $G_f = K_{Ic}^2/E$, and a_0 = .275 b were used. The c_f values examined were in the range of c_f = 9–22 mm. This length is well within the wide range of results studied by Bazant and Kazemi [20] and Shah et al. [28]. Because it is known that in the larger specimens, the process zone can fully develop, a larger value of c_f was used. Based on this approach, a $CTOD_c$ of 0.012 mm was used for the two smaller sizes and a $CTOD_c$ of 0.02 mm was used for the specimens with a depth of 320 mm. The interface bond strength of the fibers used was q_y, q_f = 4.0 and 1.6 MPa mm, respectively. A constant interface fracture toughness equal to Γ = 0.005 N/mm was used.

Results of the load versus CMOD are shown in Figure 12a, b, and c. Figure 12a represents the response of plain concrete specimens for the three sizes discussed earlier.

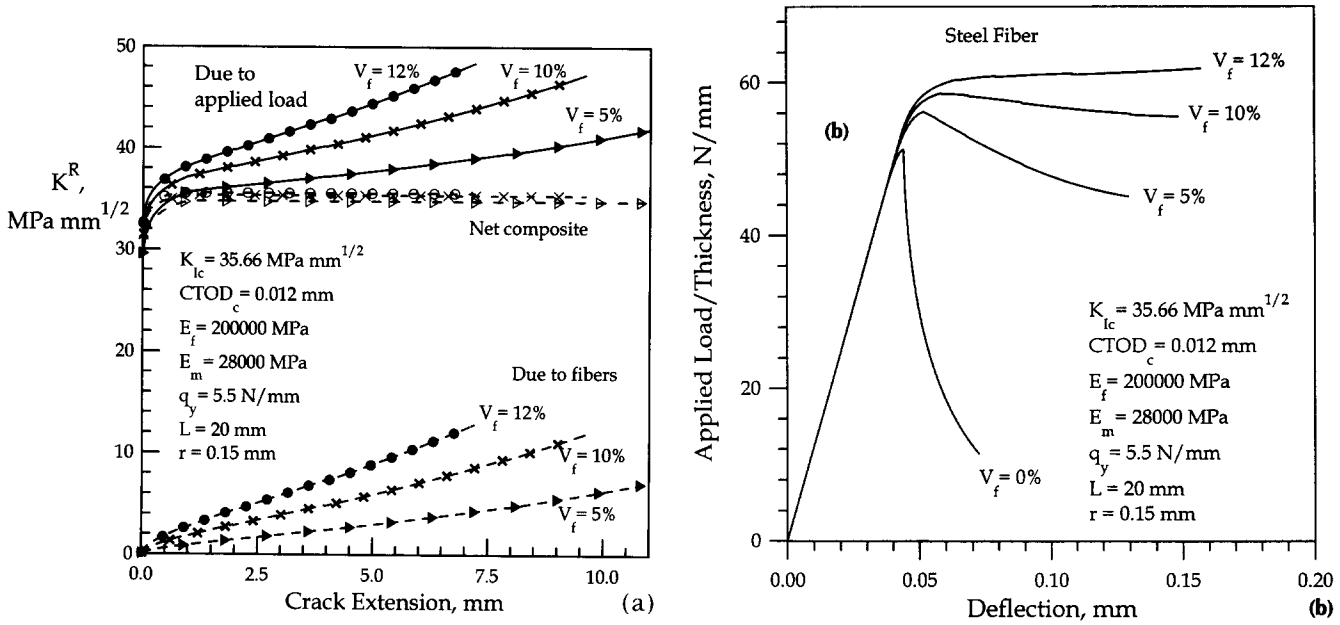

FIGURE 10. (a) K^R curves for composites with increasing fiber volume fractions. (b) The load versus deflection response. CTOD = crack tip opening displacement.

For the simulation of this model, we set the volume fraction of fibers equal to zero. The present approach underestimates the nonlinearity in the CMOD response. This is partly due to the simplifying assumptions in the model such as an assumed straight crack path and aligned fibers perpendicular to the crack path. The CMOD at the peak load was underestimated by an average of 15% using the present model. The model also underestimates the postpeak load-carrying capacity of the samples. This is partly because the dissipative mechanisms such as crack deflection and crack turtuosity are not taken into account. The predictability of the model improves with the larger size specimens. Prediction of ultimate load was achieved to within 0.3% and 3.2% of the experimental values for large and small samples, respectively.

Model prediction for size-effect study of FRC specimens with 0.5% volume fraction of straight fibers are shown in Figure 12b and 12c. Composites with 6- and 13-mm fibers are shown. The present model is capable of predicting the size effect observed in these specimens. As the size of the specimens increases, the ability of the fibers to bridge a longer process zone increases and results in more toughening contribution due to the closing pressure term.

Conclusion

A theoretical analysis is conducted by modeling the crack growth in cementitious composites reinforced with aligned short fibers. The formulation is based on an *R*-curve approach to describe the crack propagation and crack instability conditions. *R* curves of the composites are constructed by considering the fracture process zone in the cementitious matrices and the shielding contributions from the fibers in the wake region. The fiber pullout model based on fracture mechanics approach is used to provide the fiber bridging force dis-

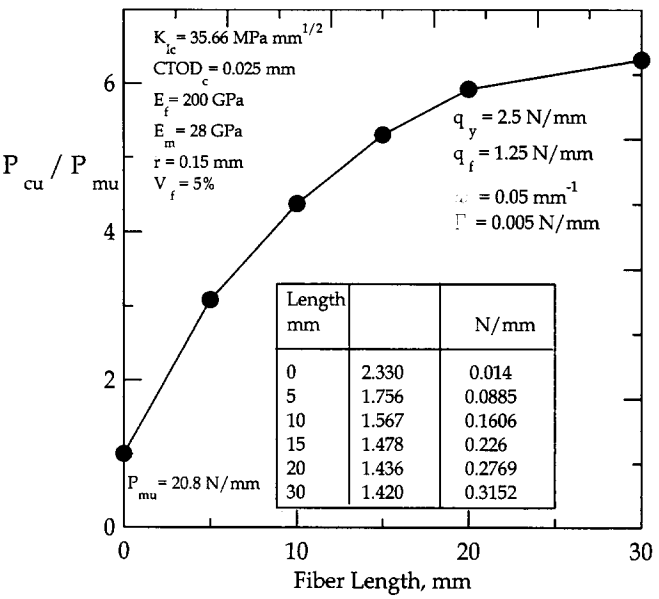

FIGURE 11. Effect of fiber length on the ultimate load. The number of fibers across the crack is held constant while the length is increased. Parameters of the *R* curve are also shown. CTOD = crack tip opening displacement.

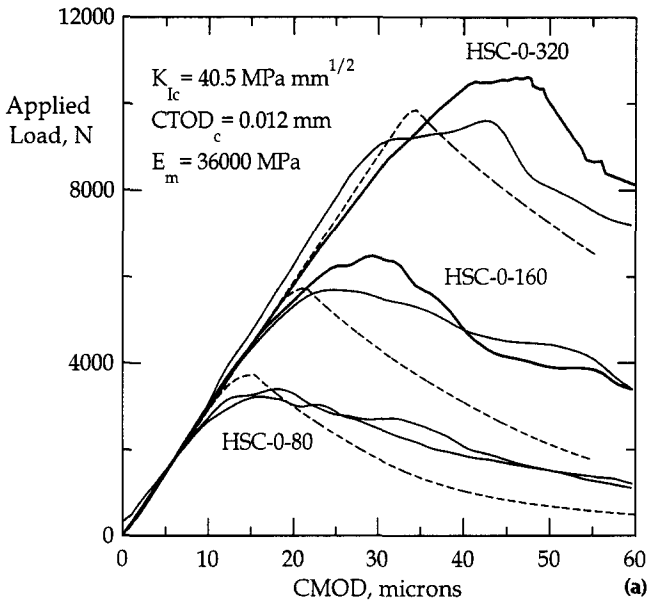

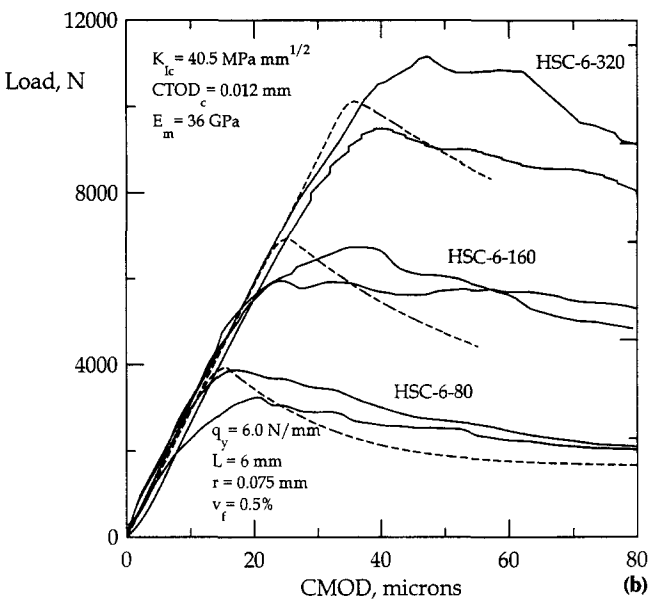

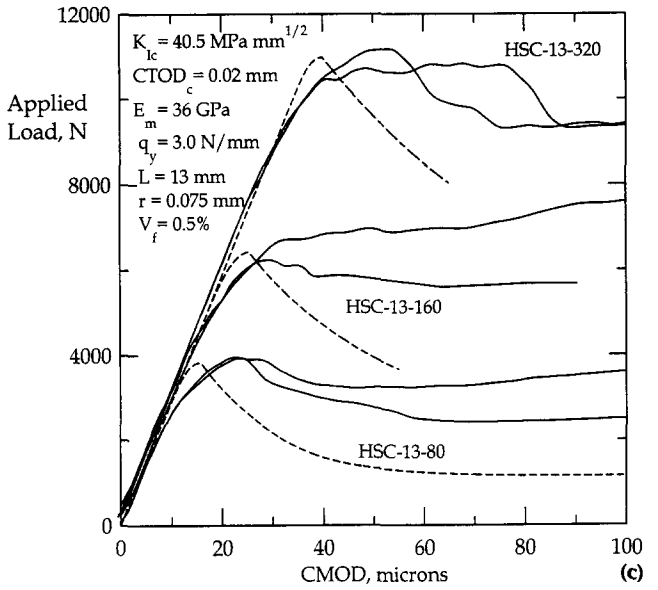

FIGURE 12. Model prediction for size-effect study of (a) plain concrete specimens, (b) fiber reinforced concrete (FRC) with $V_f = 0.5\%$ of straight fibers (L = 6 mm), and (c) FRC with V_f = 0.5% of straight fibers (L = 13 mm). Results are compared with the experimental results of Bryars et al. [26]. CTOD = crack tip opening displacement; CMOD = crack mouth opening displacement.

tributed across the main crack faces. A numerical iteration procedure is used to solve the resulting nonlinear integral equations. The effects of parameters such as fiber length, interfacial shear strength, and interfacial friction on the composite strength and toughness are studied. Results are further validated by ability of the model to predict the size effect in FRC materials.

Acknowledgments

The authors are grateful to the National Science Foundation for the Research Initiation Award No. MSM-9211063.

Appendix: The Stress Intensity Factors K_{IF} and K_{IP}

For a semiinfinite strip specimen as shown in Figure A1, the stress intensity factor due to a mutually opposite pair of unit forces acting on the crack faces at a distance x from the crack edge can be generally expressed as a function of crack length a and distance x, as:

$$K = g\left(1, \frac{x}{a}\right) = \frac{2}{\sqrt{\pi a}} \frac{G\left(\frac{x}{a}, \frac{a}{d}\right)}{\left(1 - \frac{a}{d}\right)^{3/2} \sqrt{1 - \left(\frac{x}{a}\right)^2}}$$

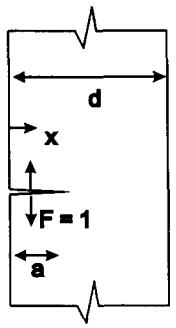

FIGURE A1. Edge crack in an infinite strip subjected to point force.

$$G\left(\frac{x}{a},\frac{a}{d}\right) = g_1\left(\frac{a}{d}\right) + g_2\left(\frac{a}{d}\right)\left(\frac{x}{a}\right) + g_3\left(\frac{a}{d}\right)\left(\frac{x}{a}\right)^2 + g_4\left(\frac{a}{d}\right)\left(\frac{x}{a}\right)^3$$

$$g_1\left(\frac{a}{d}\right) = 0.46 + 3.06\frac{a}{d} + 0.84\left(1-\frac{a}{d}\right)^5 + 0.66\left(\frac{a}{d}\right)^2\left(1-\frac{a}{d}\right)^2$$

$$g_2\left(\frac{a}{d}\right) = -3.52\left(\frac{a}{d}\right)^2$$

$$g_3\left(\frac{a}{d}\right) = 6.17 - 28.22\left(\frac{a}{d}\right) + 34.54\left(\frac{a}{d}\right)^2 - 14.39\left(\frac{a}{d}\right)^3 - \left(1-\frac{a}{d}\right)^{3/2} - 5.88\left(1-\frac{a}{d}\right)^5 - 2.64\left(\frac{a}{d}\right)^2\left(1-\frac{a}{d}\right)^5$$

$$g_4\left(\frac{a}{d}\right) = -6.63 + 25.16\left(\frac{a}{d}\right) - 31.04\left(\frac{a}{d}\right)^2 + 14.41\left(\frac{a}{d}\right)^3 + 2.0\left(1-\frac{a}{d}\right)^{3/2} + 5.04\left(1-\frac{a}{d}\right)^{5^2} + 1.98\left(\frac{a}{d}\right)^2\left(1-\frac{a}{d}\right)$$

For the distributed bridging forces $P^*(u)$ over the crack faces, assuming the unit thickness, stress intensity factor due to fibers, K_{IF}, can be obtained by integrating the distribution of the force over the crack face. The parameters are shown in Figure A2:

$$K_1^f = \int_0^a P^*(U)\, g\left(1,\frac{x}{a}\right) dx \qquad \text{(A1)}$$

where $P^*(u)$ is given by the fiber pullout solution of the differential eq 6 described previously.

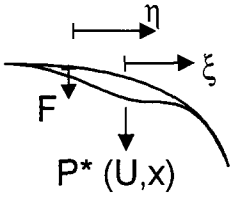

FIGURE A2. Definition of the integration parameters to calculate crack opening due to a distributed force on the crack faces.

References

1. Jenq, Y.S.; Shah, S.P. *J. Struct. Eng.* **1986,** *112,* 19–34.
2. Li, V.C.; Wu, H.C. *J. Appl. Mech. Rev.* **1992,** *45,* 390–398.
3. Li, V.C.; Leung, C.K.Y. *J. Eng. Mech.* **1992,** *118,* 2246–2264.
4. Visalvanich, K.; Naaman, A.E. *J. ACI* **1983,** *80,* 128–138.
5. Tjiptobroto, P.; Hansen, W. *ACI Mater.* **1993,** *90,* 16–25.
6. Yang, C.C.; Mura, T.; Shah, S.P. *J. Mater. Res.* **1991,** *6,* 2463–2473.
7. Li, S.H.; Shah, S.P.; Li, Z.; Mura, T. *Inter. J. Solids Struct.* **1993,** *30,* 1429–1459.
8. Mobasher, B.; Li, CY. *ACI Mater. J.* **1996,** *93,* 284–292.
9. Li, Z.; Mobasher, B.; Shah, S.P. *J. Am. Ceram. Soc.* **1991,** *74,* 2156–2164.
10. Ouyang, C.S.; Pacios, A.A.; Shah, S.P. *J. Eng. Mech. Dec.* **1994,** *120,* 2641–2659.
11. Mobasher, B.; Li, C.Y. *J. Composites Eng.* **1995,** *5,* 1349–1365.
12. Li, V.C.; Stang, H.; Krenchel, H. *J. Mater. Struct.* **1993,** *26,* 486–494
13. Gopalaratnam, V.S.; Shah, S.P. *ACI J.* **1985,** *82,* 310–323.
14. Jenq, Y.S.; Shah, S.P. *J. Eng. Mech.* **1985,** *111,* 1227–1241.
15. Ouyang, C.S.; Mobasher, B.; Shah, S.P. *Eng. Fracture Mech.* **1990,** *37,* 901–913.
16. Stang, H.; Li, Z.; Shah, S.P. *J. Eng. Mech.* **1990,** *116,* 2136–2150.
17. Steif, P.S.; Dollar, A. *J. Am. Ceram. Soc.* **1992,** *75,* 1694–1696.
18. Hoffman, J.D. *Numerical Methods for Engineers and Scientists.* McGraw-Hill: New York, 1992.
19. Ouyang, C.S.; Shah, S.P. *J. Am. Ceram. Soc.* **1991,** *74,* 2831–2836.
20. Bazant, Z.P.; Kazemi, M.T. *Int. J. Fract.* **1990,** *44,* 111–131.
21. Marshall, D.B. *Acta Metall. Mater.* **1992,** *40,* 427–441.
22. Tada, H.; Paris, P.C.; Irwin, G.R. *The Stress Analysis of Cracks Handbook* (2nd ed.). Paris Productions, Inc.: St. Louis, MO, 1985.
23. Mobasher, B.; Ouyang, C.; Shah, S.P. *Int. J. Fract.* **1991,** *50,* 199–219.
24. Aveston, A.J.; Kelly, A. *J. Mater. Sci.* **1973,** *8,* 352.
25. Romualdi, J.P.; Batson, G.B. *J. Eng. Mech.* **1963,** *89,* 147–168.
26. Bryars, L.; Gettu, R.; Barr, B.; Arino, A. In *Proceedings of Europe-US Workshop on Fracture and Damage in Quasi-Brittle Structures,* Bazant, Z.P.; Bittnar, Z.; Jirasek, M.; Mazars, J., eds. E & FN Spon: London, 1994, pp. 319–326.
27. Gettu, R.; Tabbara, M.; Bazant, Z.P. *Stress Intensity Factors for a Short Three-Point Bend Specimen,* Internal Report. Northwestern University: Evanston, IL, 1990.
28. Shah, S.P.; Swartz, S. Ouyang, C.S. *Fracture Mechanics of Concrete.* Wiley: New York, 1995.